Correlation Between In Vivo ^{18}F-FDG PET and Immunohistochemical Markers of Glucose Uptake and Metabolism in Pheochromocytoma and Paraganglioma

Anouk van Berkel*[1], Jyotsna U. Rao*[1,2], Benno Kusters[3,4], Tuna Demir[1,2], Eric Visser[5], Arjen R. Mensenkamp[6], Jeroen A.W.M. van der Laak[3], Egbert Oosterwijk[7], Jacques W.M Lenders[8,9], Fred C.G.J. Sweep[2], Ron A. Wevers[2], Ad R. Hermus[1], Johan F. Langenhuijsen[7], Dirk P.M. Kunst[10], Karel Pacak[11], Martin Gotthardt[5], and Henri J.L.M. Timmers[1]

[1]Department of Internal Medicine, Radboud University Medical Centre, Nijmegen, The Netherlands; [2]Department of Laboratory Medicine, Laboratory of Genetic, Endocrine and Metabolic Diseases, Radboud University Medical Centre, Nijmegen, The Netherlands; [3]Department of Pathology, Radboud University Medical Centre, Nijmegen, The Netherlands; [4]Department of Pathology, Maastricht University Medical Centre, Maastricht, The Netherlands; [5]Department of Nuclear Medicine, Radboud University Medical Centre, Nijmegen, The Netherlands; [6]Department of Genetics, Radboud University Medical Centre, Nijmegen, The Netherlands; [7]Department of Urology, Radboud University Medical Centre, Nijmegen, The Netherlands; [8]Department of Internal Medicine, Radboud University Medical Centre, Nijmegen, The Netherlands; [9]Department of Medicine and Institute of Clinical Chemistry and Laboratory Medicine, University Hospital Carl Gustav Carus, Dresden, Germany; [10]Department of Otolaryngology, Radboud University Medical Centre, Nijmegen, The Netherlands; and [11]Eunice Kennedy Shriver, NICHD, National Institutes of Health, Bethesda, Maryland

Pheochromocytomas and paragangliomas (PPGLs) can be localized by ^{18}F-FDG PET. The uptake is particularly high in tumors with an underlying succinate dehydrogenase (*SDH*) mutation. SDHx-related PPGLs are characterized by compromised oxidative phosphorylation and a pseudohypoxic response, which mediates an increase in aerobic glycolysis, also known as the Warburg effect. The aim of this study was to explore the hypothesis that increased uptake of ^{18}F-FDG in *SDHx*-related PPGLs is reflective of increased glycolytic activity and is correlated with expression of different proteins involved in glucose uptake and metabolism through the glycolytic pathway. **Methods:** Twenty-seven PPGLs collected from patients with hereditary mutations in *SDHB* ($n = 2$), *SDHD* ($n = 3$), *RET* ($n = 5$), neurofibromatosis 1 ($n = 1$), and myc-associated factor X ($n = 1$) and sporadic patients ($n = 15$) were investigated. Preoperative ^{18}F-FDG PET/CT studies were analyzed; mean and maximum standardized uptake values (SUVs) in manually drawn regions of interest were calculated. The expression of proteins involved in glucose uptake (glucose transporters types 1 and 3 [GLUT-1 and -3, respectively]), phosphorylation (hexokinases 1, 2, and 3 [HK-1, -2, and -3, respectively]), glycolysis (monocarboxylate transporter type 4 [MCT-4]), and angiogenesis (vascular endothelial growth factor [VEGF], CD34) were examined in paraffin-embedded tumor tissues using immunohistochemical staining with peroxidase-catalyzed polymerization of diaminobenzidine as a read-out. The expression was correlated with corresponding SUVs. **Results:** Both maximum and mean SUVs for *SDHx*-related tumors were significantly higher than those for sporadic and other hereditary tumors ($P < 0.01$). The expression of HK-2 and HK-3 was significantly higher in *SDHx*-related PPGLs than in sporadic PPGLs ($P = 0.022$ and 0.025, respectively). The expression of HK-2 and VEGF was significantly higher in *SDHx*-related PPGLs than in other hereditary PPGLs ($P = 0.039$ and 0.008, respectively). No statistical differences in the expression were observed for GLUT-1, GLUT-3, and MCT-4. The percentage anti-CD 34 staining and mean vessel perimeter were significantly higher in *SDHx*-related PPGLs than in sporadic tumors ($P = 0.050$ and 0.010, respectively). Mean SUVs significantly correlated with the expression of HK-2 ($P = 0.027$), HK-3 ($P = 0.013$), VEGF ($P = 0.049$), and MCT-4 ($P = 0.020$). **Conclusion:** The activation of aerobic glycolysis in *SDHx*-related PPGLs is associated with increased ^{18}F-FDG accumulation due to accelerated glucose phosphorylation by hexokinases rather than increased expression of glucose transporters.

Key Words: pheochromocytoma; paraganglioma; succinate dehydrogenase; Warburg effect; ^{18}F-fluorodeoxyglucose positron emission tomography

J Nucl Med 2014; 55:1253–1259
DOI: 10.2967/jnumed.114.137034

Pheochromocytomas and paragangliomas (PPGLs) are catecholamine-producing neuroendocrine tumors arising from the chromaffin cells of the adrenal medulla and extraadrenal sympathetic paraganglia. PPGLs can occur as part of hereditary syndromes. Susceptibility genes include succinate dehydrogenase (*SDH*) complex subunits and assembly factor 2 (*SDHA/B/C/D/AF2*), von Hippel-Lindau (*VHL*), *RET*, neurofibromatosis (*NF*) 1, myc-associated factor X (*MAX*), and transmembrane protein 127 (*TMEM127*) (*1*). Gene expression profiling has revealed the presence of 2 clusters of PPGLs: cluster 1 (*VHL, SDHx*), which shows increased expression of genes associated with angiogenesis and hypoxia, and cluster 2 (*RET, NF1, TMEM127,* and *MAX*), which displays a rich signature of RNA synthesis and kinase signaling (*2,3*).

Received Jan. 9, 2014; revision accepted Mar. 31, 2014.
For correspondence or reprints contact: Henri J.L.M. Timmers, Radboud University Medical Center, Department of Internal Medicine, P.O. Box 9101, 6500 HB Nijmegen, The Netherlands.
E-mail: Henri.Timmers@radboudumc.nl
*Contributed equally to this work.
Published online Jun. 12, 2014.
COPYRIGHT © 2014 by the Society of Nuclear Medicine and Molecular Imaging, Inc.

Enhanced uptake of glucose by tumor cells, compared with normal cells, is the hallmark of in vivo cancer imaging with ^{18}F-FDG PET/CT. We have shown previously that ^{18}F-FDG PET/CT is superior to other functional imaging techniques for localizing metastatic PPGL, particularly in those with an underlying *SDHB* mutation (*4–6*). ^{18}F-FDG PET/CT is also useful for localizing benign PPGLs (*7*). Interestingly, ^{18}F-FDG uptake varies among PPGLs of different genotypes, with the highest standard uptake values (SUVs) being observed in *SDH* and *VHL*-related tumors (*5,8*). The precise mechanism behind these genotype-specific differences in ^{18}F-FDG uptake has not been elucidated.

SDHx mutations cause impairment of SDH function in the mitochondrial electron transport chain and hence compromise oxidative phosphorylation (*9–11*). Abolition of SDH enzymatic activity results in activation of the hypoxic-angiogenic pathway via transcription factor hypoxia-inducible factors (HIFs)-1α and -2α (*12*). Their main target genes include genes involved in glucose metabolism (glucose transporters [GLUTs], hexokinases [HK], angiogenesis [vascular endothelial growth factor, VEGF]), survival, and motility (*13–15*). Activation of HIF-α further supports the shift of tumor cell energy metabolism from oxidative phosphorylation toward aerobic glycolysis, also known as the Warburg effect (*16*). The alternative energy-generation pathway is somewhat less efficient, requiring a much larger cellular influx of glucose to maintain the energy needs tumor cells.

High uptake of ^{18}F-FDG by *SDHx*-related tumors has been suggested to be a reflection of the Warburg effect. Various mechanisms for accelerated glucose use by tumor cells have been described. Enhanced influx of glucose via GLUTs is considered to be the most important. The overexpression of GLUT isoforms GLUT-1 and -3 is closely related to ^{18}F-FDG uptake in tumor cells (*17*). In addition, accelerated glucose phosphorylation by the cytosolic enzyme HK as the first step toward glycolysis results in enhanced ^{18}F-FDG accumulation. HK-2 is predominantly expressed in tumor cells that exhibit the Warburg effect (*18*) and is associated with elevated ^{18}F-FDG uptake in malignant conditions (*19,20*). The upregulation of both GLUTs and HK is frequently associated with malignant transformation of cells (*21*). Furthermore, activity of HK-3 and monocarboxylate transporter type 4 (MCT-4), which facilitates the cellular lactate transport, possibly is regulated by hypoxia (*10,22*). In addition, hypoxia also promotes anaerobic glycolysis, and several studies have demonstrated that ^{18}F-FDG uptake is an indirect reflection of tumor hypoxia (*23,24*).

The aim of this study was to explore the hypothesis that increased uptake of ^{18}F-FDG is reflective of increased glycolytic activity and is correlated with the expression of different proteins involved in glucose uptake and metabolism through the glycolytic pathway. Therefore, the immunohistochemical expression of GLUT-1, GLUT-3, HK-1, HK-2, HK-3, and MCT-4 was directly correlated with in vivo ^{18}F-FDG uptake in PPGLs of different genotypes. Additionally, VEGF expression, to account for hypoxia-regulated angiogenesis, and CD34, to account for genotype-specific differences in microvasculature that could alter the radiotracer supply to tumor cells, were examined.

MATERIALS AND METHODS

Patients

The study included 27 consecutive patients (17 men and 10 women; mean age ± SD, 51 ± 15 y) in whom PPGL was histopathologically confirmed and of which 22 (81%) were adrenal and 5 (19%) extra-adrenal in location. Patient characteristics are listed in Table 1 and Supplemental Table 1 (available at http://jnm.snmjournals.org). The institutional review board approved this retrospective study, and the requirement to obtain informed consent was waived.

^{18}F-FDG PET/CT Scanning

All patients underwent presurgical evaluation with ^{18}F-FDG PET/CT at the Radboud University Medical Center between December 2007 and February 2012 (Fig. 1). Patients fasted for at least 6 h before receiving a 241 ± 73 MBq dose of intravenous ^{18}F-FDG based on body weight. PET/CT scans were obtained approximately 1 h (range, 55–74 min) after injection. Before November 2011, imaging was performed using a Biograph 2 PET/CT scanner, and after November 2011 using an mCT-40 scanner (both Siemens Healthcare). Both scanners were calibrated and certified by the European Association of Nuclear Medicine (EANM) Research Ltd. in accordance with the EANM guidelines for PET/CT (*25*). First, a low-dose CT scan using CareDose with a reference of 40 mA and 130 kV was obtained from the base of the skull to the mid thigh. Instructions for breathing and positioning were given to patients. The CT transaxial matrix size was 512 × 512, with pixels of 0.98 × 0.98 mm for both scanners. CT slice width was 3 mm for the Biograph 2 and 1.5 mm for the mCT. PET images were obtained using 2-dimensional ordered-subset expectation maximization reconstruction on the Biograph 2 with 4 iterations and 16 subsets and a postreconstruction gaussian filter of 5 mm in full width at half maximum. The transaxial PET matrix size was 128 × 128, and pixel size was 5.31 × 5.31 × 3 mm. For the mCT scanner, images were obtained using time-of-flight and high-definition reconstruction with 3 iterations and 21 subsets and a postreconstruction gaussian filter of 8 mm in full width at half maximum. The transaxial PET matrix size

TABLE 1
Patients Characteristics

Genotype	No. of patients	Sex		Age (y)	Tumor location		Tumor dimensions (cm^3)
		M	F		Adrenal	Extraadrenal	
Sporadic*	15	8	7	54.2 ± 14.9	14	1	47.9 ± 56.3
SDHB	2	2	0	31.0 ± 14.1	0	2	3.4 ± 2.4
SDHD	3	2	1	49.5 ± 13.4	1	2	26.0 ± 33.8
MEN-2	5	4	1	46.8 ± 14.4	5	0	14.8 ± 21.0
NF1	1	0	1	70	1	0	51.7
MAX	1	1	0	63	1	0	20.4

*Presence of germline mutations and large deletions in SDHB/C/D, RET, VHL, and—since 2011—in SHDA, SDHAF2, TMEM127, and MAX was investigated using standard procedures, and no mutation was detected.

Study included a total of 27 patients. Data are presented as mean ± SD.

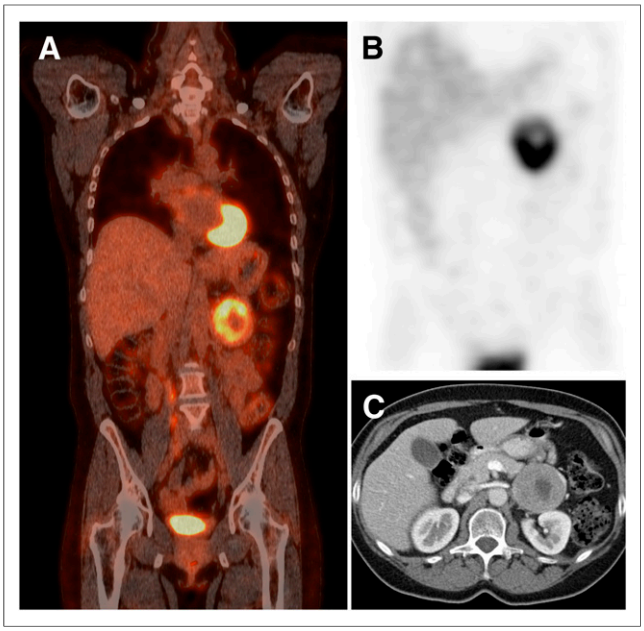

FIGURE 1. Imaging results in patient with sporadic PPGL located in left adrenal. (A) ^{18}F-FDG PET scan. (B) ^{123}I-metaiodobenzylguanidine SPECT scan. (C) CT scan.

was 256 × 256, and pixel size was 3.18 × 3.18 × 3 mm. The large value of the gaussian filter for the mCT images resulted in additional smoothing and was used to comply with the EANM guidelines for PET/CT (*25*) allowing direct comparison of quantitative data from both scanners.

Image Interpretation and Quantitative Measurements

PET/CT images were reviewed using Inveon Research Workplace software (version 4.1; Siemens Healthcare). Regions of interest were manually drawn in each transversal slice over visually assessed lesions in correspondence with CT images. Regions of interest were combined to form a volume of interest, which was used for quantitative analysis. Maximum and mean standardized uptake values (SUV_{max} and SUV_{mean}, respectively) normalized for body weight were calculated as SUV = A/IA × BW (A, activity concentration of VOI [Bq/mL]; BW, body weight [g]; IA, injected activity [Bq]). Liver-normalized standardized uptake value (SUVs) were calculated as PPGL SUVs divided by corresponding liver mean SUVs in a fixed volume of interest in the upper central liver. All calculated SUVs were-decay corrected using the following formula: $A_0 = A_t \times e^{\lambda t}$ (A_0, corrected activity; A_t, uncorrected activity; λ, decay constant [ln2/110] min^{-1}; t, elapsed time in min).

Immunohistochemical Staining and Quantification and Quantitative Polymerase Chain Reaction (qPCR)

Information for immunohistochemical staining and quantification and qPCR is given in the supplemental material.

Statistical Analysis

Statistical analysis was conducted using SPSS 20 (SPSS Inc.) and GraphPad Prism 6 software (GraphPad Inc.). For comparison of immunohistochemical staining scores and SUVs of different genotypes, scores and SUVs were analyzed using the Kruskal–Wallis test with the post hoc Dunn test. Results are presented as mean ± SD. Correlations were examined using the Spearman correlation test. A 2-side *P* value of less than 0.05 was considered to be statistically significant.

RESULTS

^{18}F-FDG Uptake in PPGLs

The SUV_{max} of PPGLs ranged from 0.8 to 11.8 (3.7 ± 3.2) and SUV_{mean} from 0.6 to 5.4 (1.8 ± 1.5) ($r = 0.91$, $P < 0.001$). The distribution of SUVs in PPGLs across hereditary and sporadic tumors is shown in Figure 2. The SUV_{max} for hereditary-cluster-1 tumors (*SDHB*, *SDHD*) was higher (9.6 ± 1.5) than for hereditary-cluster-2 tumors (*RET*, *NF1*, *MAX*: 1.9 ± 0.3, $P < 0.01$) and sporadic tumors (2.6 ± 1.7, $P < 0.01$). Also, SUV_{mean} for hereditary-cluster-1 tumors was higher (4.5 ± 0.8) than for hereditary-cluster-2 (1.0 ± 0.1, $P < 0.01$) and sporadic tumors (1.3 ± 0.8, $P < 0.01$).

SUV_{max} was higher for adrenal (2.7 ± 1.8, $P < 0.001$) and extraadrenal PPGLs (8.2 ± 4.3, $P < 0.01$) than for normal adrenal glands (1.2 ± 0.5). Also, SUV_{mean} was higher for adrenal (1.3 ± 0.8, $P < 0.01$) and extraadrenal PPGL (4.0 ± 1.9, $P < 0.01$) than for normal adrenal glands (0.8 ± 0.2). ^{18}F-FDG uptake by normal adrenal glands did not exceed that of the liver in any case. No false-positive lesions were observed on ^{18}F-FDG PET/CT.

The volume of the PPGL lesions was calculated as described before (*26*) and varied from 0.8 to 161 cm^3 (35 ± 46). There was no significant relation between tumor volume and ^{18}F-FDG uptake ($P = 0.945$).

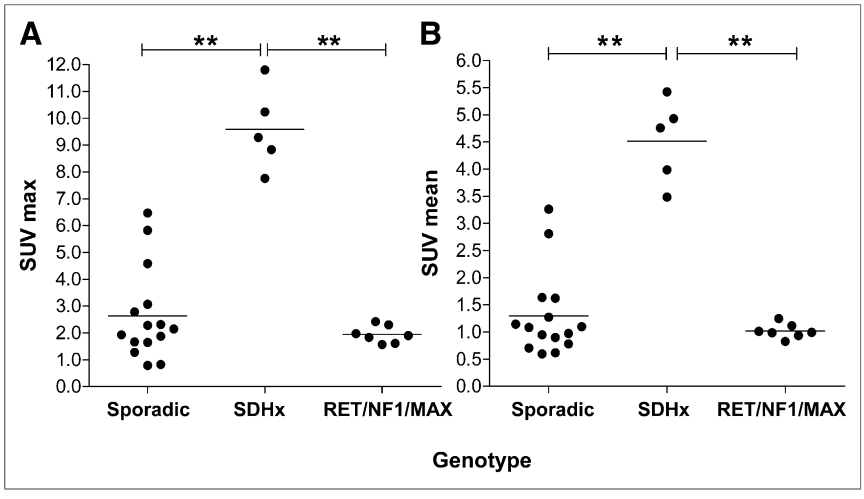

FIGURE 2. ^{18}F-FDG PET SUV in PPGLs across different genotypes. (A) SUV_{max}. (B) SUV_{mean}. All SUVs are normalized for body weight and liver and corrected for decay. $^{**}P < 0.01$.

Markers of Glucose Uptake and Metabolism

All 27 PPGL samples showed a positive cytoplasmic staining for HK-1. Staining was high across samples (Fig. 3), and no significant differences were observed between the different genotypes and sporadic samples (Fig. 4).

HK-2 staining showed a clear variation between samples (Fig. 3). Negative to occasionally medium cytoplasmic staining was encountered in sporadic tumor samples. HK-2 expression was found to be significantly higher in *SDHx*-related PPGLs than in sporadic ($P = 0.022$) and *RET*-, *NF1*-, and *MAX*-related tumors ($P = 0.039$) (Fig. 4). An increased expression of HK-2 was confirmed at the messenger RNA (mRNA) level using qPCR, and a high ($P = 0.004$)

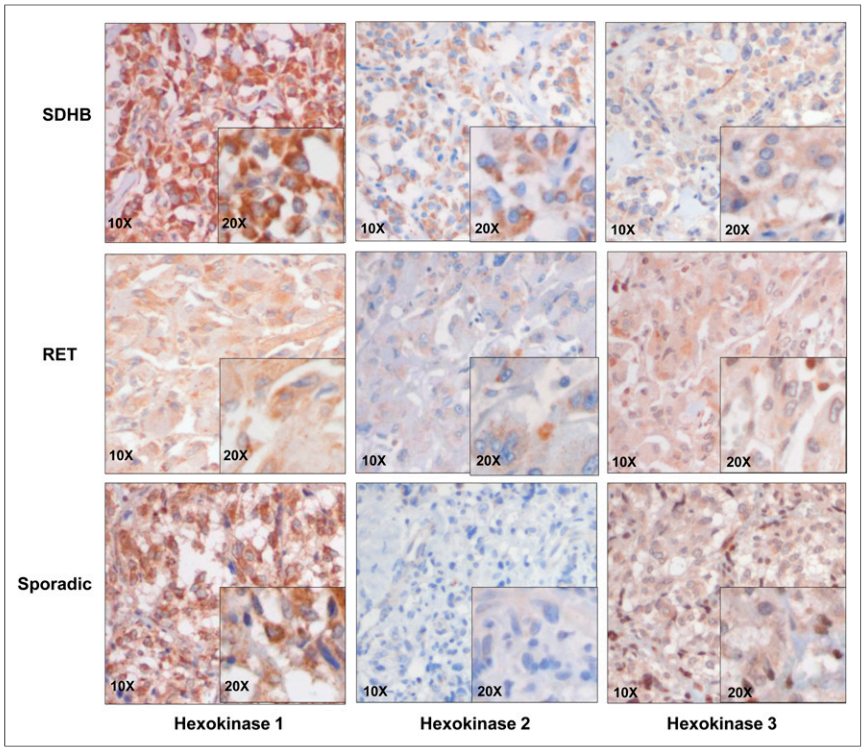

FIGURE 3. Immunohistochemical staining of PPGLs for hexokinases. Representative images of *SDHB, RET,* and sporadic tumor with magnifications as indicated. Areas with brown color (diaminobenzidine polymer) are representative of positive staining.

expression of the markers was observed in *SDHx*-related tumors when compared with sporadic tumors and cluster-2–related tumors (Supplemental Fig. 1). HK-3 expression was significantly higher in *SDHx*-related PPGLs than in sporadic tumors ($P = 0.025$); however, when compared with *RET*-, *NF1*-, and *MAX*-related tumors no statistical significance was observed (Fig. 4).

GLUT-1 and GLUT-3 showed predominantly cytoplasmic staining and occasionally (5%–10%) cell membrane staining (Fig. 5). Sporadic and *SDHx*-, *RET*-, *NF1*-, and *MAX*-related tumors showed an overall similar GLUT-1 expression (Fig. 6). A homogeneous distribution of staining in the cytoplasm was observed. Sporadic and *RET*-associated tumors showed a similar GLUT-3 expression, which was usually scored as medium. *SDHx*-related PPGLs appeared to exhibit a higher GLUT-3 staining than sporadic and *RET* PPGLs. However, statistical significance was not achieved (Fig. 6). On the other hand, at the mRNA level, GLUT-3 expression did not show significant differences between the groups (Supplemental Fig. 1). MCT-4 was localized to cytoplasm as well as membrane. The expression of MCT-4 did not show significant differences between the different genotypes (Figs. 5 and 6). VEGF expression was found to be significantly higher in *SDHx*-related PPGLs than in *RET*-, *NF1*-, and *MAX*-related PPGLs ($P = 0.008$) (Figs. 5 and 6). There was a significant difference in mean percentage anti-CD34–stained area ($P = 0.050$) and mean vessel perimeter ($P = 0.010$) between *SDHx*-related and sporadic PPGLs. The microvessel density did not differ among genotypes.

Relationship Between ^{18}F-FDG Uptake and Markers of Glucose Uptake and Metabolism

The correlative relationships between immunohistochemical staining and calculated SUVs and corresponding *P* values are summarized in Table 2. The SUV_{mean} of PPGLs was significantly associated with HK-2, HK-3, VEGF, and MCT-4 staining. The strongest correlation with SUV was found for HK-3 expression ($R = 0.471$, $P = 0.013$). No significant relationship was found between GLUT-1 and GLUT-3 staining and SUV. SUV_{max} showed only a significantly correlative relationship for HK-2 ($R = 0.409$, $P = 0.034$) and HK-3 immunohistochemical staining ($R = 0.381$, $P = 0.050$). No correlative relationships were found for ^{18}F-FDG uptake and vessel parameters.

DISCUSSION

We examined the ex vivo expression of markers of the Warburg effect in PPGLs using immunohistochemical staining and their correlation with uptake of in vivo ^{18}F-FDG on PET/CT scans. We confirmed genotype-specific differences in ^{18}F-FDG uptake for which *SDHx*-related PPGLs showed highest SUVs. The expression of HK-2 was significantly higher in *SDHx*-related PPGLs

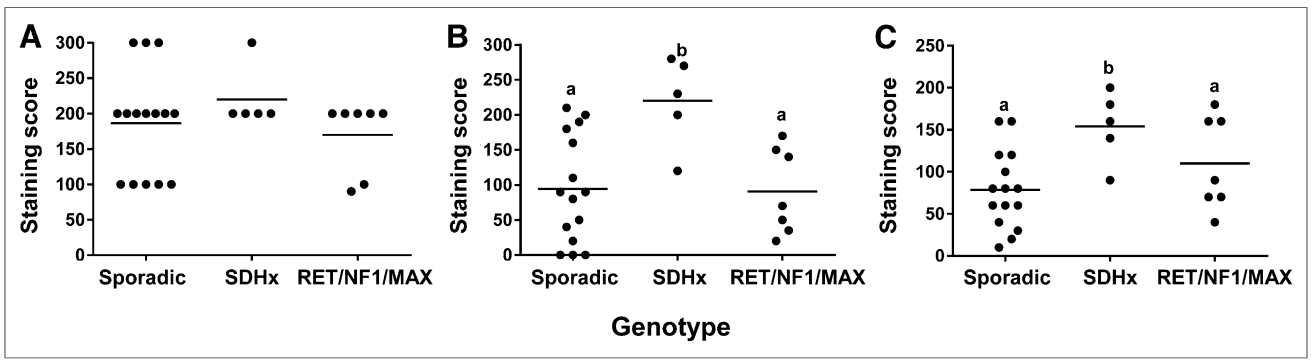

FIGURE 4. Comparison of staining for HK-1 (A), HK-2 (B), and HK-3 (C) among different PPGL genotypes. Graphs represent staining scores, calculated as percentage area stained positive times staining intensity. Groups with different letters as superscripts are significantly different.

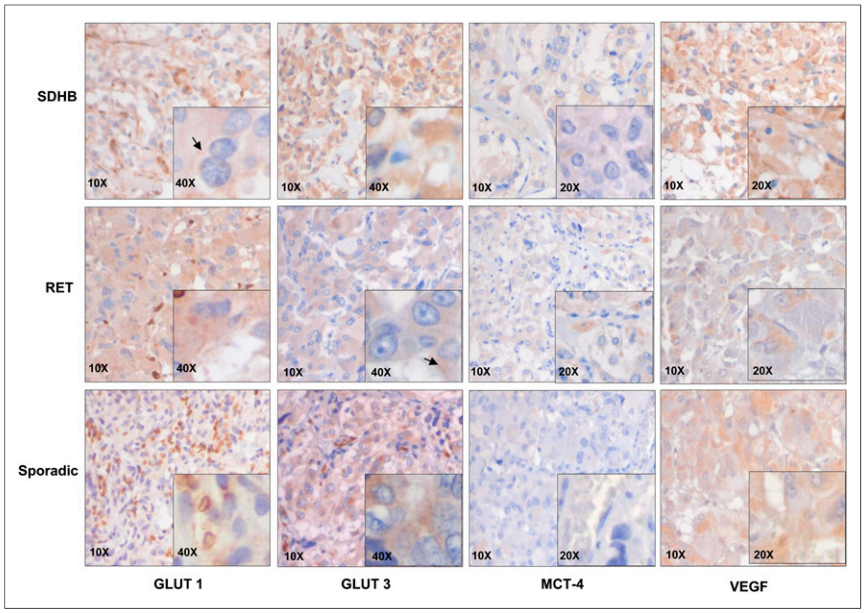

FIGURE 5. Immunohistochemical staining of PPGLs for GLUT-1 and GLUT-3, MCT-4, and VEGF. Representative images of *SDHB, RET,* and sporadic tumor with magnifications as indicated. Areas with brown color (diaminobenzidine polymer) are representative of positive staining.

than in sporadic and cluster-2 PPGLs. Furthermore, the expression of HK-3 was significantly higher in *SDHx*-related PPGLs than in sporadic PPGLs, and expression of VEGF was significantly higher in *SDHx*-related PPGLs than in cluster-2 PPGLs. The uptake of ^{18}F-FDG significantly correlated with the expression of HK-2, HK-3, VEGF, and MCT-4.

Similar to glucose, ^{18}F-FDG is taken up by tumor cells mostly via facilitative transport by GLUTs. After cell entry, ^{18}F-FDG is phosphorylated by HKs into ^{18}F-FDG-6-P, which, in contrast to glucose-6-P, cannot be further metabolized along the glycolytic pathway. The cell membrane is impermeable to ^{18}F-FDG-6-P, so it accumulates within cells directly proportionate to their metabolic activity. ^{18}F-FDG-6-P can theoretically escape from the cell by dephosphorylation back to ^{18}F-FDG by glucose-6-phosphatase. In general, this process is negligible because of the low intracellular levels of the dephosphorylating enzyme. Therefore, ^{18}F-FDG uptake of any cell is determined by expression of GLUTs and activity of HKs. Another possible determinant is tumoral blood flow, which brings ^{18}F-FDG to the cell and reasonably increases its metabolism in parallel. However, activation of the hypoxic-angiogenic pathway via HIF-1α and -2α results in adaptation of the tumor to a hypoxic environment and consequently an uncoupling of blood flow and metabolism, implying hypoxic stimulation of glucose metabolism in the presence of adequate oxygen. This phenomenon, known as the Warburg effect (*27*), characterizes cluster-1 PPGLs (*VHL*, *SDHx*). Favier et al. demonstrated that HIF-2α, which together with HIF-1α upregulates VEGF and GLUT-1 gene expression (*28*), is overexpressed in *VHL*- and *SDHx*-related PPGLs (*10*). VEGF activated in endothelial vascular cells within tumors can significantly contribute to ^{18}F-FDG uptake (*29*).

High SUVs observed in *SDHx*-related PPGLs could be related to the Warburg effect and thus we expected to find a stronger GLUT-1 and GLUT-3 expression in *SDHx*- than in cluster-2–related PPGLs. However, we found no significant increase in immunohistochemical GLUT staining in *SDHx*-related tumors. We observed a predominantly cytoplasmic and weak membrane staining for both GLUT-1 and GLUT-3 as also reported by Blank et al. (*30*). In addition, we found no correlation between GLUTs and SUVs in PPGLs. Taken together, these results suggest that glucose uptake may not be preferentially regulated by GLUT-1 and GLUT-3 in these tumors. Aloj et al. concluded that higher levels of GLUT protein do not guarantee increased ^{18}F-FDG uptake by cancer cells (*31*). Differences in ^{18}F-FDG uptake may be caused by differences in GLUT activity rather than by differences in number of transporters present. Also, our findings suggest that the expression and recruitment of GLUTs to the cell membrane do not appear to vary in a genotype-specific way.

Instead of GLUT, higher ^{18}F-FDG uptake in *SDHx* PPGLs might be related to expression of HKs. HK-2 showed an increased expression in *SDHx*-related PPGLs as predicted. The expression of HK-2 is regulated by HIF-1, and it is predominantly overexpressed in various cancer cells that display the Warburg effect (*18*) and is associated with ^{18}F-FDG uptake (*20,32*). Favier et al. (*10*) also observed a significantly higher HK-2 gene expression in *SDHx*-related PPGLs than in *NF1*- and *RET*-related PPGLs. Immunohistochemical staining of HK-3 showed increased expression in *SDHx*-related PPGLs, compared with sporadic tumors, but when compared with cluster-2 tumors no significant increased expression was found. In addition, we found a stronger correlation between HK-3 and SUV_{mean} than HK-2 and SUV_{mean}. A study using rat hepatoma cell line N1S1 reported the role of hypoxia signaling in the regulation of HK-3 (*22*). However, little is known about its regulation by HIFs in PPGLs. Thus, increased glucose phosphorylation by HKs rather than the glucose transport by GLUTs is reflected as increased ^{18}F-FDG uptake. Also, we assessed expression of HK-1 and observed lack of differences among different genotypes as it is a housekeeping enzyme ubiquitously expressed in mammalian tissues independent of HIF and is unaltered in most cancer cells (*33*).

TABLE 2
Correlations Between ^{18}F-FDG Uptake and Immunohistochemical Markers of Glucose Uptake and Metabolism

	SUV_{max}		SUV_{mean}	
Marker	*R*	*P*	*R*	*P*
HK-2	0.409	0.034*	0.425	0.027*
HK-3	0.381	0.050*	0.471	0.013*
GLUT-1	−0.001	0.998	−0.100	0.620
GLUT-3	0.174	0.386	0.263	0.185
VEGF	0.312	0.114	0.383	0.049*
MCT-4	0.373	0.055	0,444	0.020*

All SUVs are normalized to liver and decay-corrected. Correlations are expressed as Spearman ρ and *P* value (*$P < 0.05$).

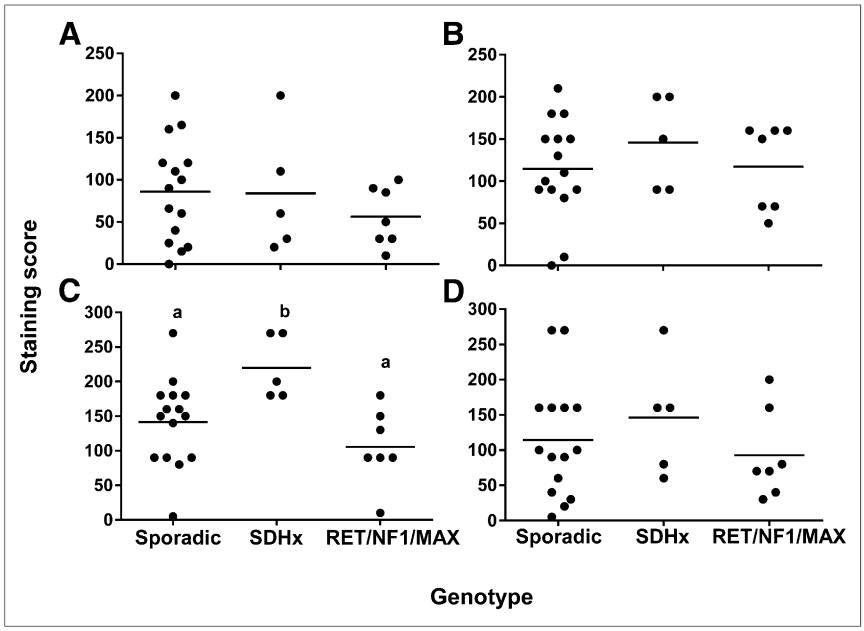

FIGURE 6. Comparison of staining for GLUT-1 (A), GLUT-3 (B), VEGF (C), and MCT-4 (D) among different PPGL genotypes. Graphs represent staining scores, calculated as percentage area stained positive times staining intensity. Groups with different letters as superscripts are significantly different.

Increase in HK-2 and HK-3 expression in *SDHx*-related PPGLs points toward increased glycolysis, which we further investigated by assessing the expression of MCT-4. This monocarboxylate transporter exports lactate out of the cell, and its expression is known to be high in cells with increased glycolysis and lactate production. We found membrane and cytoplasmic staining for MCT-4, but the levels of expression did not vary among the different genotypes. However, Favier et al. (*10*) reported an increased expression of MCT-4 at the mRNA level in *SDHx*-related tumors. Thus, though evidence suggests increased glycolysis in *SDHx*-related tumors, it might not be accompanied by increased lactate production.

We determined the expression of VEGF to further explore our hypothesis that higher ^{18}F-FDG uptake in *SDHx*-related PPGLs is reflective of the Warburg effect. A significantly increased expression of VEGF was observed, suggesting an increase in microvessel density in *SDHx*-related PPGLs. These results are in line with our previous estimations of mRNA levels measured by qPCR (*34*) and with Blank et al. (*30*) who also observed a significant correlation between *SDHB*-related PPGLs and microvessel density. VEGF stimulates angiogenesis, but this probably will not necessarily result in higher uptake of ^{18}F-FDG because newly formed vessels can be leaky and do not provide tumor cells with nutrients such as glucose. Therefore, we also investigated CD34, a marker for more mature endothelial cells. An increase in percentage of anti-CD34 staining was confirmed by quantitative analysis of CD34 immunohistochemical staining. Moreover, mean vascular perimeter was significantly higher in *SDHx*-related tumors than in cluster-2 and sporadic tumors. Nevertheless, no statistical differences in microvessel density were observed, which could be attributed to highly heterogeneous vascular patterns observed in these tumors. Taken together, increased endothelial surface area in this type of tumors can potentially contribute to higher accumulation of ^{18}F-FDG, supporting the idea that functionality of vessels is more critical for SUVs than microvessel density.

Additional studies with a larger sample size are needed to further explore the genotype-specific signature of expression of markers of the Warburg effect and their impact on functional imaging of these tumors. Also, somatic mutations in apparently sporadic tumors will need to be considered. Besides genetic factors, the influence of the microenvironment on the metabolism of tumor cells deserves further investigations. Furthermore, besides immunohistochemistry, a more quantitative approach such as Western blotting (not performed in the present study because of limited sample quantity) would be useful for a better assessment of the expression of the investigated markers. In addition, SUVs merely provide a semiquantitative measurement of ^{18}F-FDG uptake not information on the actual exchange of ^{18}F-FDG between the intra- and extracellular compartment. This would require a dynamic scanning approach. In addition, considering the heterogeneous uptake pattern observed in some tumors, both SUV_{mean} and SUV_{max} have their limitations regarding their representativeness for the tumor as a whole and the correlation with tissue markers.

CONCLUSION

Activation of aerobic glycolysis in *SDHx*-related PPGLs is associated with increased ^{18}F-FDG accumulation due to accelerated glucose phosphorylation by hexokinases rather than increased expression of glucose transporters. Differences in tumor vasculature and the activity of transporter systems may also contribute to genotype-related SUVs.

DISCLOSURE

The costs of publication of this article were defrayed in part by the payment of page charges. Therefore, and solely to indicate this fact, this article is hereby marked "advertisement" in accordance with 18 USC section 1734. Financial support was granted by the European Union Seventh Framework Programme (FP7/2007-2013) under grant agreement no. 259735 (ENSAT CANCER). No other potential conflict of interest relevant to this article was reported.

ACKNOWLEDGMENTS

We acknowledge Mirjam de Weijert for help with arranging laboratory needs for immunostaining and Prof. Otto Boerman for discussion on the selection of markers studied and help in setting up the pilot experiments.

REFERENCES

1. Gimenez-Roqueplo AP, Dahia PL, Robledo M. An update on the genetics of paraganglioma, pheochromocytoma, and associated hereditary syndromes. *Horm Metab Res.* 2012;44:328–333.
2. Eisenhofer G, Huynh TT, Pacak K, et al. Distinct gene expression profiles in norepinephrine- and epinephrine-producing hereditary and sporadic pheochromocytomas: activation of hypoxia-driven angiogenic pathways in von Hippel-Lindau syndrome. *Endocr Relat Cancer.* 2004;11:897–911.

3. López-Jiménez E, Gomez-Lopez G, Leandro-Garcia LJ, et al. Research resource: Transcriptional profiling reveals different pseudohypoxic signatures in SDHB and VHL-related pheochromocytomas. *Mol Endocrinol.* 2010;24:2382–2391.
4. Timmers HJ, Chen CC, Carrasquillo JA, et al. Comparison of ^{18}F-fluoro-L-DOPA, ^{18}F-fluoro-deoxyglucose, and ^{18}F-fluorodopamine PET and ^{123}I-MIBG scintigraphy in the localization of pheochromocytoma and paraganglioma. *J Clin Endocrinol Metab.* 2009;94:4757–4767.
5. Timmers HJ, Chen CC, Carrasquillo JA, et al. Staging and functional characterization of pheochromocytoma and paraganglioma by ^{18}F-fluorodeoxyglucose (^{18}F-FDG) positron emission tomography. *J Natl Cancer Inst.* 2012;104:700–708.
6. Timmers HJ, Kozupa A, Chen CC, et al. Superiority of fluorodeoxyglucose positron emission tomography to other functional imaging techniques in the evaluation of metastatic SDHB-associated pheochromocytoma and paraganglioma. *J Clin Oncol.* 2007;25:2262–2269.
7. Taieb D, Sebag F, Barlier A, et al. ^{18}F-FDG avidity of pheochromocytomas and paragangliomas: a new molecular imaging signature? *J Nucl Med.* 2009;50:711–717.
8. Blanchet EM, Gabriel S, Martucci V, et al. F-FDG PET/CT as a predictor of hereditary head and neck paragangliomas. *Eur J Clin Invest.* 2014;44:325–332.
9. Gimenez-Roqueplo AP, Favier J, Rustin P, et al. Functional consequences of a SDHB gene mutation in an apparently sporadic pheochromocytoma. *J Clin Endocrinol Metab.* 2002;87:4771–4774.
10. Favier J, Briere JJ, Burnichon N, et al. The Warburg effect is genetically determined in inherited pheochromocytomas. *PLoS ONE.* 2009;4:e7094.
11. Rao JU, Engelke UF, Rodenburg RJ, et al. Genotype-specific abnormalities in mitochondrial function associate with distinct profiles of energy metabolism and catecholamine content in pheochromocytoma and paraganglioma. *Clin Cancer Res.* 2013;19:3787–3795.
12. Jochmanová I, Yang C, Zhuang Z, Pacak K. Hypoxia-inducible factor signaling in pheochromocytoma: turning the rudder in the right direction. *J Natl Cancer Inst.* 2013;105:1270–1283.
13. Gordan JD, Simon MC. Hypoxia-inducible factors: central regulators of the tumor phenotype. *Curr Opin Genet Dev.* 2007;17:71–77.
14. Dahia PL, Familial Pheochromocytoma C. Transcription association of VHL and SDH mutations link hypoxia and oxidoreductase signals in pheochromocytomas. *Ann N Y Acad Sci.* 2006;1073:208–220.
15. Selak MA, Armour SM, MacKenzie ED, et al. Succinate links TCA cycle dysfunction to oncogenesis by inhibiting HIF-alpha prolyl hydroxylase. *Cancer Cell.* 2005;7:77–85.
16. Warburg O. On the origin of cancer cells. *Science.* 1956;123:309–314.
17. Macheda ML, Rogers S, Best JD. Molecular and cellular regulation of glucose transporter (GLUT) proteins in cancer. *J Cell Physiol.* 2005;202:654–662.
18. Mathupala SP, Ko YH, Pedersen PL. Hexokinase-2 bound to mitochondria: cancer's stygian link to the "Warburg Effect" and a pivotal target for effective therapy. *Semin Cancer Biol.* 2009;19:17–24.
19. Ahn KJ, Hwang HS, Park JH, et al. Evaluation of the role of hexokinase type II in cellular proliferation and apoptosis using human hepatocellular carcinoma cell lines. *J Nucl Med.* 2009;50:1525–1532.
20. Yamada T, Uchida M, Kwang-Lee K, et al. Correlation of metabolism/hypoxia markers and fluorodeoxyglucose uptake in oral squamous cell carcinomas. *Oral Surg Oral Med Oral Pathol Oral Radiol.* 2012;113:464–471.
21. de Geus-Oei LF, van Krieken JH, Aliredjo RP, et al. Biological correlates of FDG uptake in non-small cell lung cancer. *Lung Cancer.* 2007;55:79–87.
22. Wyatt E, Wu R, Rabeh W, Park HW, Ghanefar M, Ardehali H. Regulation and cytoprotective role of hexokinase III. *PLoS ONE.* 2010;5:e13823.
23. Dierckx RA, Van de Wiele C. FDG uptake, a surrogate of tumour hypoxia? *Eur J Nucl Med Mol Imaging.* 2008;35:1544–1549.
24. Clavo AC, Brown RS, Wahl RL. Fluorodeoxyglucose uptake in human cancer cell lines is increased by hypoxia. *J Nucl Med.* 1995;36:1625–1632.
25. Boellaard R, O'Doherty MJ, Weber WA, et al. FDG PET and PET/CT: EANM procedure guidelines for tumour PET imaging: version 1.0. *Eur J Nucl Med Mol Imaging.* 2010;37:181–200.
26. Eisenhofer G, Pacak K, Huynh TT, et al. Catecholamine metabolomic and secretory phenotypes in phaeochromocytoma. *Endocr Relat Cancer.* 2011;18:97–111.
27. Vander Heiden MG, Cantley LC, Thompson CB. Understanding the Warburg effect: the metabolic requirements of cell proliferation. *Science.* 2009;324:1029–1033.
28. Semenza GL. Hypoxia-inducible factors in physiology and medicine. *Cell.* 2012;148:399–408.
29. Maschauer S, Prante O, Hoffmann M, Deichen JT, Kuwert T. Characterization of ^{18}F-FDG uptake in human endothelial cells in vitro. *J Nucl Med.* 2004;45:455–460.
30. Blank A, Schmitt AM, Korpershoek E, et al. SDHB loss predicts malignancy in pheochromocytomas/sympathethic paragangliomas, but not through hypoxia signalling. *Endocr Relat Cancer.* 2010;17:919–928.
31. Aloj L, Caraco C, Jagoda E, Eckelman WC, Neumann RD. Glut-1 and hexokinase expression: relationship with 2-fluoro-2-deoxy-D-glucose uptake in A431 and T47D cells in culture. *Cancer Res.* 1999;59:4709–4714.
32. Watanabe Y, Suefuji H, Hirose Y, et al. ^{18}F-FDG uptake in primary gastric malignant lymphoma correlates with glucose transporter 1 expression and histologic malignant potential. *Int J Hematol.* 2013;97:43–49.
33. Wolf A, Agnihotri S, Micallef J, et al. Hexokinase 2 is a key mediator of aerobic glycolysis and promotes tumor growth in human glioblastoma multiforme. *J Exp Med.* 2011;208:313–326.
34. Span PN, Rao JU, Oude Ophuis SB, et al. Overexpression of the natural antisense hypoxia-inducible factor-1α transcript is associated with malignant pheochromocytoma/paraganglioma. *Endocr Relat Cancer.* 2011;18:323–331.